

PSR B1951+32: A Bow Shock-Confined X-ray Nebula, a Synchrotron Knot and an Optical Counterpart Candidate

D.-S. Moon^{1,2,3}, J.-J. Lee⁴, S. S. Eikenberry^{3,5}, B.-C. Koo⁴, S. Chatterjee^{3,6},
D. L. Kaplan⁷, J. J. Hester⁸, J. M. Cordes³, Y. A. Gallant^{9,10}, L. Koch-Miramond¹⁰

ABSTRACT

The radio pulsar B1951+32 and the supernova remnant CTB 80 provide a rich laboratory for the study of neutron stars and supernova remnants. Here, we present ground-based optical and near-infrared observations of them, along with X-ray observations with *Chandra* and a re-analysis of archival data obtained with the *Hubble Space Telescope*. The X-ray observations reveal a cometary pulsar wind nebula which appears to be confined by a bow shock produced by high-velocity motion of the pulsar, making PSR B1951+32 a rare pulsar exhibiting both an H α bow shock and a shocked X-ray pulsar wind nebula. The distribution of H α and radio continuum emission is indicative of a contact discontinuity of the shocked pulsar winds and shocked ambient medium at ~ 0.05 pc. On the other hand, the optical synchrotron knot of PSR B1951+32 likely has a flat spectrum in the optical and near-infrared wavebands, and our astrometry is consistent with only one of the two reported optical counterpart candidates for the pulsar.

¹Robert A. Millikan Fellow, Division of Physics, Mathematics and Astronomy, Caltech, MC 103-33, Pasadena, CA 91125

²Space Radiation Laboratory, Caltech, MC 220-47, Pasadena, CA 91125; moon@srl.caltech.edu

³Department of Astronomy, Cornell University, Ithaca, NY 14853; cordes@astro.cornell.edu

⁴Astronomy Program, SEES, Seoul National University, Seoul 151-742, Korea; jjlee@astro.snu.ac.kr , koo@astrohi.snu.ac.kr

⁵Department of Astronomy, University of Florida, Gainesville, FL 32611; eiken@astro.ufl.edu

⁶Jansky Fellow, National Radio Astronomy Observatory, Socorro, NM 87801; schatter@aoc.nrao.edu

⁷Department of Astronomy, Caltech, MC 105-24, Pasadena, CA 91125; dlk@astro.caltech.edu

⁸Department of Physics and Astronomy, Arizona State University, Tempe, AZ 85287; jhester@asu.edu

⁹Groupe d'Astroparticules, Université Montpellier II, 34095 Montpellier Cedex 5, France; gallant@gamum2.in2p3.fr

¹⁰DAPNIA/Service d'Astrophysique, CEA/Saclay, 91191 Gif-sur-Yvette Cedex, France; lkoch@discover.y.saclay.cea.fr

Subject headings: pulsars: individual (PSR B1951+32) — shock waves — stars: neutron — supernova remnants: individual (CTB 80)

1. Introduction

Rotation-powered pulsars (RPPs) exhibit diverse interesting phenomena ranging from periodic pulsations to supersonic motions through the interstellar medium, as well as relativistic winds often revealed by interaction with the neighborhood. More than 30 years after the discovery of RPPs, however, the origins for many of these phenomena still remain out of our grasp, although there has been a recent surge of development in some of these fields, largely driven by new X-ray satellites typified by *Chandra*. One of the many unprecedented features of the new X-ray satellites is superb angular resolutions; for example, *Chandra* gives $\lesssim 1''$ accuracy in the positions of X-ray sources, comparable to the typical optical and near-infrared (IR) observations. This enables high-precision comparative studies of X-ray and optical/near-IR results, such as more robust searches for optical/near-IR counterparts to RPPs and multi-wavelength studies of their close vicinity.

In many ways, the ~ 39.5 ms radio pulsar PSR B1951+32 (Kulkarni et al. 1988) in the CTB 80 supernova remnant (SNR) provides a rare opportunity to study the interesting phenomena of RPPs. It is a moderately young pulsar of 1.1×10^5 yrs spin-down age, which is comparable to, but slightly larger than, the age determined by its proper motion (6.4×10^4 yrs; Migliazzo et al. 2002) and the dynamical age of CTB 80 (7.7×10^4 yrs; Koo et al. 1990), indicating a finite initial spin. The measured proper motion (25 ± 4 mas yr $^{-1}$) corresponds to a velocity of 240 ± 40 km s $^{-1}$ at 2 kpc, moving away from the SNR center. In the optical, PSR B1951+32 is located in a $\sim 1'$ nebular core emitting both Balmer-dominated and forbidden lines. Hester & Kulkarni (1988, 1989) suggested that the core is a bow shock formed by the relativistic winds from the pulsar when it encountered the material behind a radiative shock of the SNR. *ROSAT* X-ray observations were also suggestive of the pulsar wind nature of the core, albeit its inadequate spatial resolution (Safi-Harb et al. 1995). On the other hand, using archival data from the *Hubble Space Telescope* (HST), Hester (2000) reported a possible optical synchrotron knot near PSR B1951+32, and Butler et al. (2002) claimed the detection of its two optical counterpart candidates. However, the lack of color information and rather large astrometric uncertainties make it difficult to reach any further conclusion on their nature.

In this *Letter*, we present X-ray and optical/near-IR observations of PSR B1951+32, searching for the predicted X-ray pulsar wind nebula in the optical core, as well as the emission from the claimed optical synchrotron knot and counterpart candidates.

2. Observations and Results

The CTB 80 core was observed with *Chandra* on 2001 July 12 for a total good time of 78.2 ks using its Advanced CCD Imaging Spectrometer (S3 chip), with a custom sub-array mode of 192 rows, minimizing pile-up on the pulsar while still imaging the entire core. Figure 1 shows a resulting X-ray image, where a strong point source (i.e., PSR B1951+32; $\sim 21,900$ photon counts) is embedded in diffuse emission. Its position is (19:52:58.23, +32:52:41.0) with $0''.02$ uncertainties¹ in each coordinate (J2000). Considering the $0''.6$ systematic uncertainty of the *Chandra* astrometry, the X-ray position is consistent with that inferred from pulsar radio timing (Foster et al. 1994). Additionally, several other point sources were detected in the *Chandra* image, and Table 1 lists four of them which have isolated counterparts in the 2MASS point source catalog. The offsets between their *Chandra* and 2MASS coordinates are smaller than $0''.7$, comparable to the combined systematic uncertainty of the *Chandra* and 2MASS astrometry. (The systematic uncertainty of the 2MASS astrometry is $0''.2$.)

We observed PSR B1951+32 on 2001 July 16 with the 2048×2048 pixel CCD of Carnegie Observatories Spectrograph and Multi-object Imaging Camera (COSMIC) on the 5-m Palomar Hale telescope. We used *g* (500 nm), *r* (655 nm), and *i* (800 nm) broad-band filters with 100 s integration time for each band, and proceeded with the standard data reduction, such as bias/dark-subtractions and flat-fielding. We next used ~ 100 2MASS point sources and the IRAF task *ccmap* to obtain $0''.28$ (RA) and $0''.40$ (DEC) astrometric uncertainties of the COSMIC images. We also performed K_s band ($2.15 \mu\text{m}$) observations with the Keck I telescope on 2003 November 6 using Near-IR Camera (NIRC) equipped with a 256×256 pixel InSb detector. We obtained 18 dithered frames, each with 42 s integration time, and subtracted dark and median-combined sky frames. We then shifted and combined them to make a final image. In addition, we re-analyzed archival data for CTB 80 from Wide Field and Planetary Camera 2 aboard HST on 1997 October 2. We used ~ 10 2MASS point sources to obtain the astrometric solutions for the NIRC and HST images with IRAF *ccmap*.

Figure 2 compares the $\text{H}\alpha$ (HST F656N band; 2.2 nm wide at 656.4 nm) image of the CTB 80 core with the X-ray image. In order to match them, we undertook the following procedure. *First*, we tied the *Chandra* image to the COSMIC images using the point sources in Table 1, which gave $0''.25$ uncertainty in each coordinate (see the following paragraph for a detailed description). *Next*, we replaced the COSMIC image with the HST F656N band image. The astrometric discrepancy of them was estimated to be $0''.24$; therefore, the two images in Figure 2 were matched with $0''.35$ uncertainty. In the bottom panel, we identify a $\sim 40''$ cometary X-ray nebula, elongated along the proper motion of PSR B1951+32 with

¹All positional uncertainties quoted in this *Letter* represent the 90% confidence levels.

the pulsar at the head. The tail shows diffuse and extended emission in the northeast, where the pulsar has traveled. The south-western boundary of the nebula appears to be confined by a bow shock-like feature in $H\alpha$, and the X-ray emission shows a steep gradient in the confined region. Figure 3 presents the distribution of the X-ray and $H\alpha$ emission along the proper motion of PSR B1951+32 (i.e., the arrow in the bottom panel of Figure 2), showing that the $H\alpha$ emission peaks $\sim 7''$ ahead of the pulsar in the direction of its proper motion.

Figure 4 shows the COSMIC *gri*, HST F547 (48.6 nm wide at 547.9 nm), and NIRC K_s band images centered on PSR B1951+32. In the COSMIC images, we determined the pulsar position in two different ways. *First*, we simply found its *Chandra* position in the COSMIC astrometry with $0''.53$ (RA) and $0''.60$ (DEC) uncertainties, dominated by the systematic astrometric uncertainties of *Chandra* and 2MASS and by uncertainties in the COSMIC astrometry. The large dotted circle in Figure 4(f) represents the position of PSR B1951+32 determined in this way. *Secondly*, the *Chandra* image was tied to the COSMIC images using the X-ray point sources and their 2MASS counterparts in Table 1, where the (intrinsic) X-ray positional uncertainties of the point sources and the uncertainties of the COSMIC astrometry dominate the final uncertainties of $0''.25$ in each coordinate. The small outlined circle in Figure 4(f) represents the position of PSR B1951+32 determined in this way. The positions of the two claimed optical counterpart candidates (i.e., 1HST and 4HST; Butler et al. 2002) are shown in Figure 4(f) – while 1HST is within the error circle, 4HST is outside.

The optical synchrotron knot of PSR B1951+32 reported by Hester (2000) was identified in the HST F547M band image in Figure 4(e). Given $E(B-V) \simeq 0.8$ extinction towards PSR B1951+32 (Hester & Kulkarni 1989), the extinction-corrected magnitude of the knot is 20.1 ± 0.2 ($= [3.3 \pm 0.7] \times 10^{-5}$ Jy) in the F547M band. The knot was also clearly detected in the *r* and K_s bands (Figure 4b,d), with estimated extinction-corrected magnitudes of 20.0 ± 0.2 ($= [4.5 \pm 1.4] \times 10^{-5}$ Jy) and 18.1 ± 0.2 ($= [3.9 \pm 0.7] \times 10^{-5}$ Jy), respectively. (The quoted uncertainties represent the 68.3% confidence levels.) However, emission associated with the knot was not detected in the HST data obtained with narrow-band line filters of F502N (2.7 nm wide at 502.3 nm), F656N, and F673N (4.7 nm wide at 673.2 nm).

3. Discussion and Conclusions

Previous optical and X-ray observations showed that PSR B1951+32 has likely been interacting with the recombining material behind the radiative shock of the CTB 80 SNR, likely forming a bow shock in the core (e.g., Hester & Kulkarni 1989; Safi-Harb et al. 1995). The radio continuum images resemble our *Chandra* image, together with a feature reminiscent of a bow shock (e.g., Migliazzo et al. 2002). In Figure 2–3, the $H\alpha$ emission overlaps the

X-ray emission in the core (especially in the eastern part), and, around PSR B1951+32, it also shows a bow shock-like feature confining the cometary X-ray nebula. One simple interpretation of the overall emission of the CTB 80 core (except for the bow shock-associated features around PSR B1951+32; see below) is that the X-ray and radio emission represent the synchrotron radiation of relativistic pulsar winds, while the $H\alpha$ emission does cooling, recombining thermal plasma shocked by them (e.g., Hester & Kulkarni 1989). Note that this still allows the existence of $H\alpha$ emission purely associated with the CTB 80 SNR, which might be responsible for the $H\alpha$ emission in the western lobes of the CTB 80 core apparently lacking the X-ray and/or radio counterparts, different from one in the eastern part.

Obviously, the most distinctive new feature of the CTB 80 core is the cometary X-ray nebula headed by PSR B1951+32 along its proper motion, seemingly confined by the $H\alpha$ emission forming bow-shock morphology at $\sim 7''$ ahead of the pulsar (Figure 2). The revelation of such a feature is in good accordance with the previous interpretation of the CTB 80 core (e.g., Hester & Kulkarni 1989), in which the cometary X-ray nebula represents the shocked pulsar winds confined by an $H\alpha$ bow shock formed by collisional excitation of the ambient medium via supersonic motion of PSR B1951+32. For this, it is important to note that there is a significant contribution of collisional excitation to the $H\alpha$ emission in the CTB 80 core (in addition to the recombination mentioned above; Hester & Kulkarni 1989), which is supportive of the bow-shock interpretation. One interesting result is that the distance (from the pulsar) to the $H\alpha$ bow shock ($\sim 7''$) is larger than the value ($\sim 3''$) obtained for the radio bow shock (Migliazzo et al. 2002; Chatterjee & Cordes 2002), indicating the location of a contact discontinuity of the inner and outer shocks between them, with the radio emission representing the inner shock (or shocked pulsar winds). Assuming $5''$ to be the projected angular distance to the contact discontinuity, we obtain ~ 0.05 pc at 2 kpc.

In order to have the bow shock formed, ram pressure balance is required between the relativistic pulsar winds and the ambient medium: $\rho_a v_{\text{psr}}^2 \simeq \dot{E}/4\pi\Omega cr_s^2$, where ρ_a is the ambient medium density, v_{psr} the pulsar velocity, \dot{E} the pulsar spin-down energy, $4\pi\Omega$ the solid angle through which the pulsar winds flow, c the speed of the light, and r_s the stagnation radius. Assumption of equipartition between the pressure of magnetic field and of particle near the bow shock leads to $B_{\text{eq}}(\mu\text{G}) \sim 50(n_{\text{H}}/\text{cm}^3)^{1/2}(v_{\text{psr}}/100 \text{ km s}^{-1})$, where n_{H} is the hydrogen number density, and also to $B_{\text{eq}}(\mu\text{G}) \sim 200\Omega^{-1/2}(\dot{E}/10^{36} \text{ ergs s}^{-1})^{1/2}(r_s/0.01 \text{ pc})^{-1}$. The observed values $v_{\text{psr}} \simeq 240 \text{ km s}^{-1}$, $\dot{E} \simeq 3.7 \times 10^{36} \text{ ergs s}^{-1}$, and $r_s \simeq 0.03 \text{ pc}$ ($\simeq 3''$) of PSR B1951+32, as well as $\Omega < 1$, estimate that $B_{\text{eq}} > 100 \mu\text{G}$. This reconciles with Hester & Kulkarni (1989) which estimated the preshock density and magnetic field to be $\sim 50 \text{ cm}^{-3}$ and $\sim 600 \mu\text{G}$. For $B_{\text{eq}} = 600 \mu\text{G}$, $\Omega < 0.1$, corresponding to highly anisotropic pulsar winds. If we assume that $B > 100 \mu\text{G}$ in the entire cometary X-ray nebula, its synchrotron cooling time is $t_{\text{sync}}(\text{yrs}) \sim 40E_{\text{keV}}^{-1/2} (B/100 \mu\text{G})^{-3/2} < 40 \text{ yrs}$, where E_{keV} is the observed

photon energy in keV. Considering the size ($\sim 20''$) of the cometary X-ray nebula and the magnitude of the PSR B1951+32 proper motion ($\sim 25 \text{ mas yr}^{-1}$), the short cooling time indicates that the cometary X-ray nebula has likely been replenished by the relativistic pulsar winds flowing from the pulsar. Note that similar results have recently been reported for other pulsar wind nebulae (Kaspi et al. 2001; Gaensler et al. 2003). In conclusion, after the millisecond (recycled) pulsar PSR B1957+20 (Stappers et al. 2003), PSR B1951+32 is only a second pulsar showing both inner and outer shocks in a pulsar wind nebula, and it is a unique pulsar exhibiting such a feature in the optical, X-ray, and radio emission together.

Our results confirm that the claimed optical synchrotron knot of PSR B1951+32 is indeed a continuum source in nature. In Figure 4, the emission from the knot appears to be present in the all five broad bands (although its significance is weak in the g and i bands). For the HST data, the knot is visible only in the relatively line-free F547M band image (Figure 4[e]), while it is absent in the narrow-band line filter images (i.e., F502N, F656N, and F673N). Thus, the knot exhibits continuum emission with a flat spectrum in the optical and near-IR wavebands (see § 2 for the flux estimation), unless it has a significant variability. The Crab pulsar is also known to have a similar optical synchrotron knot (Hester et al. 1995) which might be caused by quasi-stationary shocks from pulsar polar outflows (Lou 1998). On the other hand, of the two optical counterpart candidates for PSR B1951+32 (Butler et al. 2002), our improved astrometry is consistent only with 1HST (while it excludes 4HST; Figure 4). However, it is possible that 1HST simply represents non-uniformity in the optical synchrotron knot or emission from any background star. We need multi-epoch, multi-color observations to study the synchrotron knot and optical counterpart more thoroughly.

Part of data presented herein were obtained at the W. M. Keck Observatory, which is operated by the California Institute of Technology (CIT), the University of California, and NASA. This research is based on the data from the archive at STScI, which is operated by the association of Universities for Research in Astronomy, Inc. under the NASA contract NAS 5-26555. This research has also made use of the data products from the Two Micron All Sky Survey, which is a joint project of the University of Massachusetts and IPAC/CIT, funded by NASA and NSF. DSM was supported in part by an NSF grant AST-9986898 and also by a Millikan fellowship at CIT; JJJ was supported by a KOSEF grant ABRL 3345-20031017. SSE is supported by an NSF CAREER award AST-0328522; SC is supported by a Jansky fellowship from NRAO. DLK is supported by a fellowship from the Fannie and John Hertz Foundation; YAG was supported in part by EC fellowship HPMFCT-2000-00671.

REFERENCES

- Butler, R. F., Golden, A., & Shearer, A. 2002, *A&A*, 395, 845
- Chatterjee, S., & Cordes, J. M. 2002, *ApJ*, 575, 407
- Foster, R. S., Lyne, A. G., Shemar, S. L., & Backer, D. C. 1994, *AJ*, 108, 175
- Gaensler, B. M., van der Swaluw, E., Camilo, F., Kaspi, V. M., Baganoff, F. K., Yusef-Zadeh, F., & Manchester, R. N. 2003, *ApJ* submitted, preprint (astro-ph/0312362)
- Hester, J. J., et al. 1995, *ApJ*, 448, 240
- Hester, J. J. 2000, *AAS*, 197, 8216
- Hester, J. J. & Kulkarni, S. 1988, *ApJ*, 331, L121
- . 1989, *ApJ*, 340, 362
- Kaspi, V. M., Gotthelf, E. V., Gaensler, B. M., & Lyutikov, M. 2001, *ApJ*, 562, L163
- Koo, B.-C., Reach, W. T., Heiles, C., Fesen, R. A., & Shull, J. M. 1990, *ApJ*, 364, 178
- Kulkarni, S. R., Clifton, T. R., Backer, D. C., Foster, R. S., Fruchter, A. S., & Taylor, J. H. 1988, *Nature*, 331, 50
- Lou, Y. -Q. 1998, *MNRAS*, 294, 443
- Migliazzo, J. M., Gaensler, B. M., Backer, D. C., Stappers, B. W., van der Swaluw, E., & Strom, R. G. 2002, *ApJ*, 567, L141
- Safi-Harb, S., Ögelman, H., & Finley, J. P. 1995, *ApJ*, 439, 772
- Stappers, B. W., Gaensler, B. M., Kaspi, V. M., van der Klis, M., & Lewin, W. H. G. 2003, *Science*, 299, 1372

Table 1. Parameters of the X-ray Point Sources

List	Coordinates (J2000) ^a		<i>Chandra</i> Counts	2MASS Magnitudes		
	<i>Chandra</i> ^b	2MASS		<i>J</i>	<i>H</i>	<i>K_s</i>
1	(53:11.88[2], 53:11.7[4])	(53:11.89, 53:11.4)	17.3	12.3	12.2	12.1
2	(53:08.21[3], 53:10.3[2])	(53:08.23, 53:10.3)	47.0	13.2	12.7	12.6
3	(52:49.21[2], 52:42.1[3])	(52:49.22, 52:42.0)	19.1	12.1	11.9	11.8
4	(52:47.97[2], 52:47.9[4])	(52:47.97, 52:47.2)	24.8	13.2	12.9	13.0

^aThe values are offsets from (19:00:00, +32:00:00).

^bThe numbers in brackets represent statistical uncertainties at the 90 % confidence level in the last quoted digit.

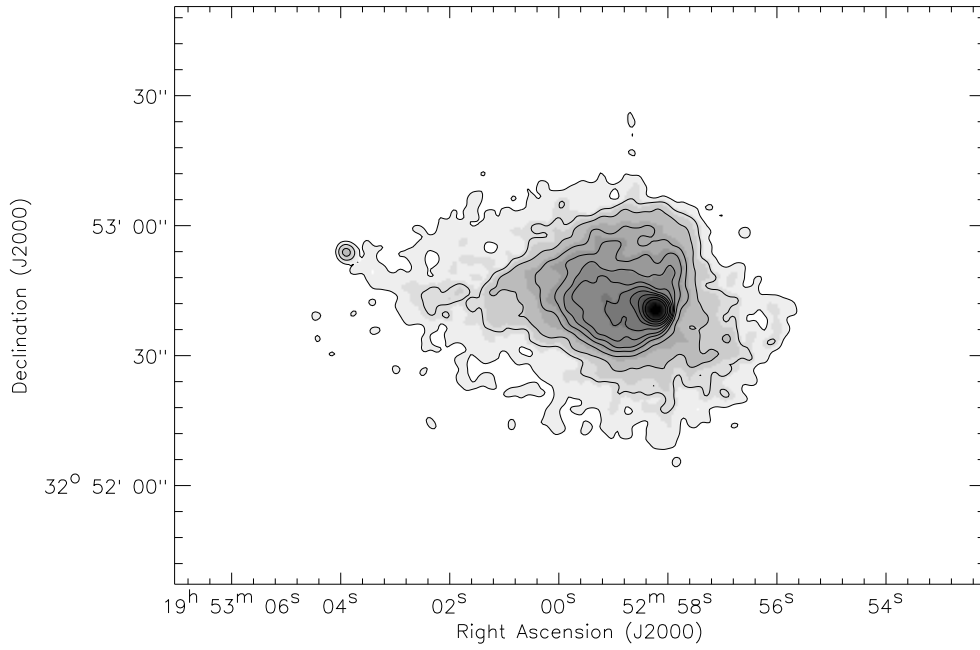


Fig. 1.— *Chandra* X-ray (0.3–10 keV) image (both in grey scale and contour) of the CTB 80 core. The image was convolved with a Gaussian filter of 1" FWHM. The contour levels correspond to 0.1, 0.2, 0.4, 0.8, 1.1, 1.5, 1.9, 2.6, 3.8, 5.7, 10.5, and 19 % of the peak brightness.

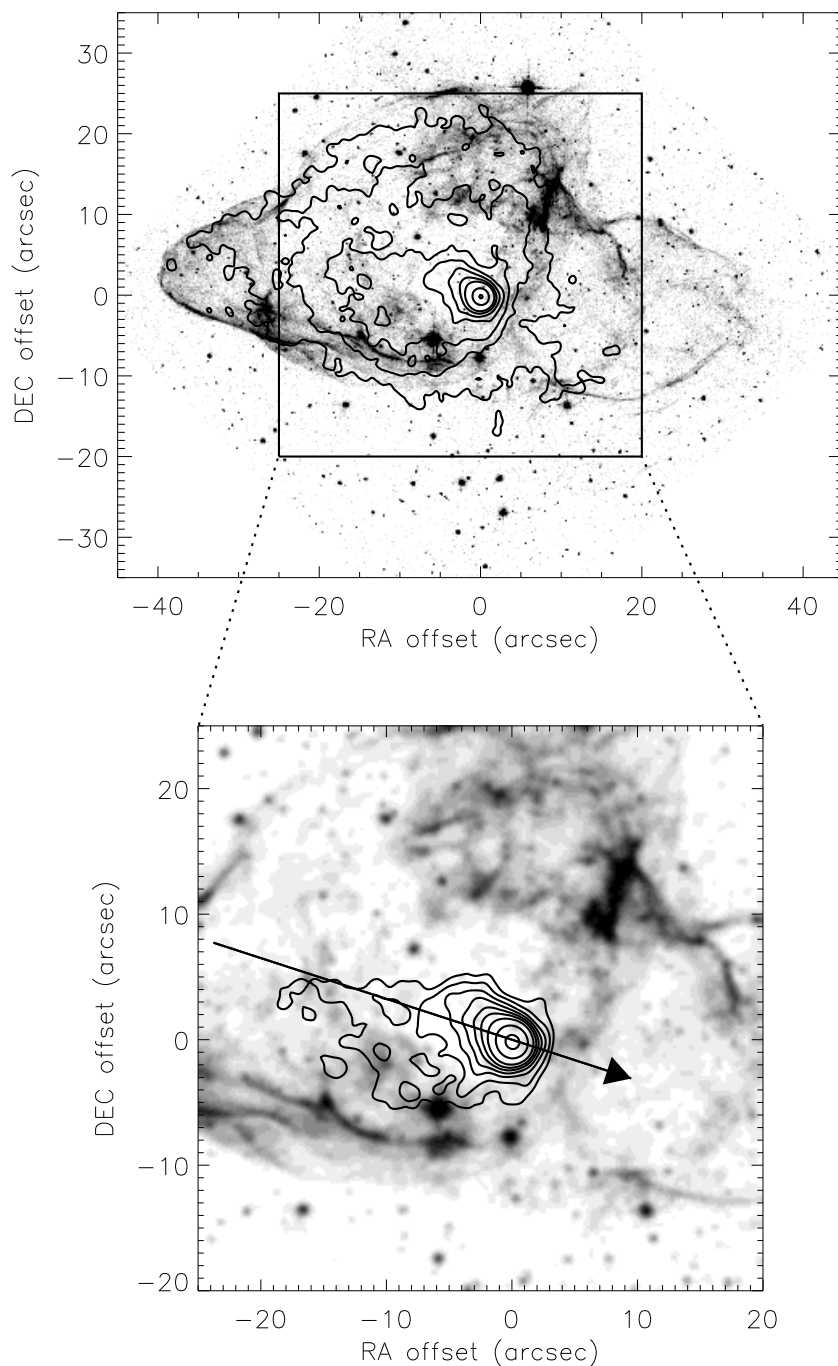


Fig. 2.— *Chandra* X-ray image (contour) superimposed on the $H\alpha$ image obtained with the HST F656N filter (grey scale). The axes represent the offsets from the pulsar position. The contour levels are 0.1, 0.4, 0.7, 1.3, 2.2, 4.0, 7.3, 36.6, and 95.2 % of the peak brightness for the upper panel; 0.9, 1.2, 1.6, 2.2, 3.1, 4.4, 7.3, 22.0, and 73.2 % for the bottom panel. The HST image was convolved with a Gaussian filter of $0''.4$ FWHM. The arrow in the bottom panel shows the direction of the the proper motion of PSR B1951+32 (Migliazzo et al. 2002).

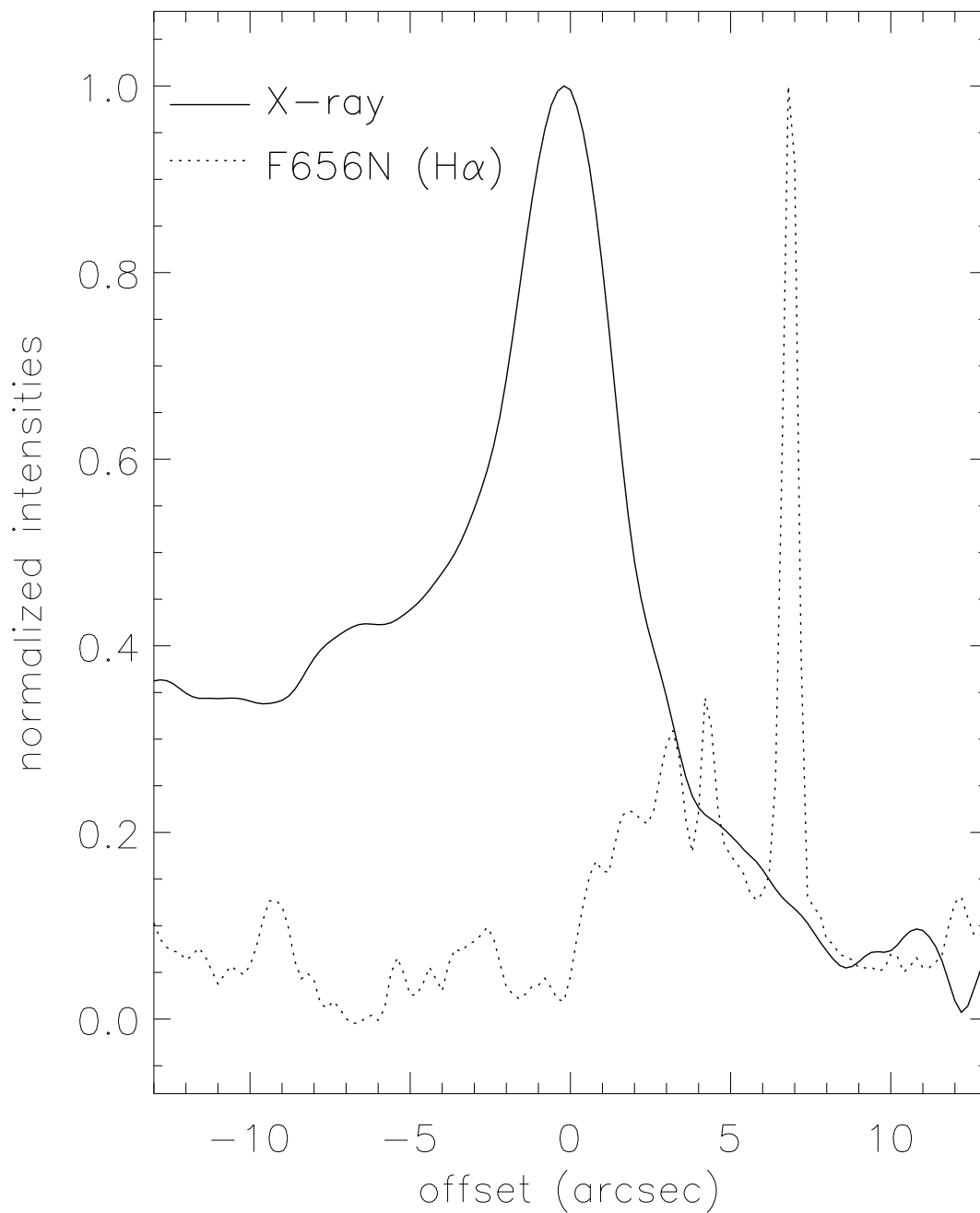


Fig. 3.— Distribution of the normalized intensities of the X-ray (solid) and H α (dotted) emission in Figure 2 along the proper motion (i.e., the arrow) of PSR B1951+32. The X-ray emission is normalized in the logarithmic scale; the H α emission in the linear scale. The intensities are calculated by bilinear interpolation at regularly spaced points on the arrow. The x-axis represents the offsets from the pulsar, with negative for the northeast direction.

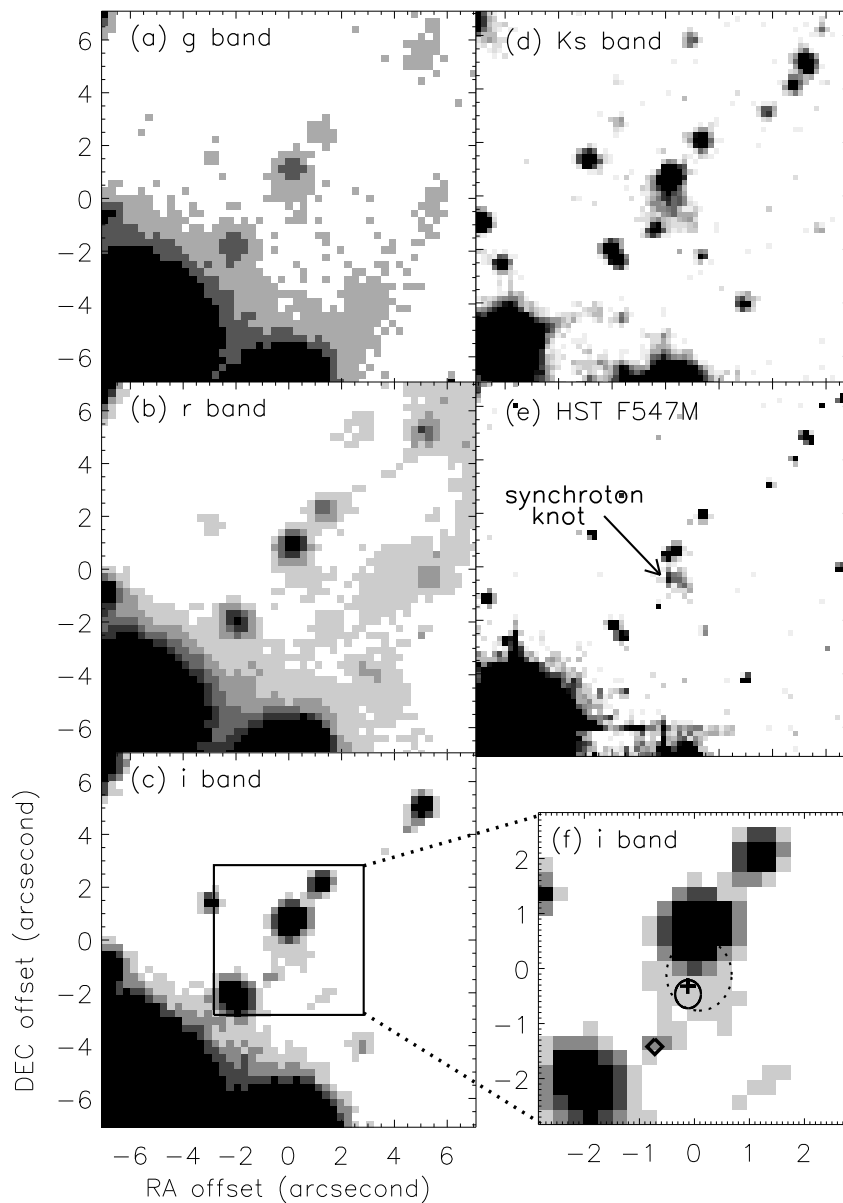


Fig. 4.— (a–c): COSMIC *gri*-band images around PSR B1951+32. (d–e): NIRC K_s band and HST F547M band images. The arrow in (e) points to the optical synchrotron knot. (f): A magnified view of (c). The dotted and outlined circles represent the positional uncertainties (90 % confidence level) of PSR B1951+32, determined from absolute astrometry and image alignment, respectively. The cross and diamond correspond to 1HST and 4HST, respectively.